Japanese Journal of Applied Physics **56**, 07JF04 (2017)
https://doi.org/10.7567/JJAP.56.07JF04

REGULAR PAPER

Mechanism of synchronized change in ultrasonic integrated backscatter across human heart wall

Yumi Tobinai[1], Hirofumi Taki[2,1], and Hiroshi Kanai[1,2*]

[1]*Graduate School of Engineering, Tohoku University, Sendai 980-8579, Japan*
[2]*Graduate School of Biomedical Engineering, Tohoku University, Sendai 980-8579, Japan*

*E-mail: kanai@ecei.tohoku.ac.jp

Received November 25, 2016; accepted February 15, 2017; published online June 2, 2017

Ultrasonic integrated backscatter (IB) from the heart wall, which has been employed for quantitative tissue characterization of the myocardium, is known to have cyclic variation-a decrease in systole and an increase in diastole. In the present study, by tracking the measurement position of the myocardium and compensating for the movement due to the heartbeat, IB and its temporal variation were obtained from the same site with a high temporal resolution of 1.73 ms. In an in vivo study on a healthy subject, the temporal variation of IB values homogeneously changed across the heart wall, especially during the slow filling and the atrial systole phases. This new finding shows that the IB value reflects a small movement of the myocardium of about 5 mm/s. Thus, the proposed measurement has a potential for quantitative and accurate evaluation of the contraction and relaxation of the myocardium.

1. Introduction

Ultrasonic diagnosis is non-invasive and inexpensive, and has thus been widely used in the diagnosis of heart disease. In patients with a history of myocardial infraction and hypertrophic cardiomyopathy, echogenicity of the diseased heart wall is increased in ultrasonic B- and M-mode images.[1,2)] Therefore, several approaches have been reported that use the ultrasound image brightness pattern for the diagnosis of the heart disease. In addition, these approaches have also been used in the evaluation of the change in thickness of the heart wall,[3)] blood flow measurement of the cardiac lumen by the ultrasonic Doppler method,[4)] and measurement of the left ventricular ejection fraction.[5)] These methods are suitable for evaluating the structure, blood flow, and movement of the heart. However, it is necessary to improve their accuracy to detect pathological changes in the tissue. Therefore, more accurate and quantitative tissue characterization of the myocardium using ultrasound imaging is desired.

Ultrasonic integrated backscatter (IB) from the heart wall, which reflects myocardial deformation at a wavelength of about 500 μm,[6,7)] is obtained by averaging the ultrasonic scattering power of the returned signal from a region in the tissues. Several research studies have shown that an increase in IB and ultrasonic attenuation of the myocardium has a high correlation with the density of the collagen fibers.[8–10)]

Madaras et al. found that IB from the normal myocardium shows cyclic variation-a decrease in systole and an increase in diastole during one cardiac cycle.[11)] Wickline et al. explained the cyclic variation of IB using a Maxwell model that consists of three elements: the contractile element inside myocardial cells, and the elastic elements inside and outside cells arranged in a series-parallel configuration representing the physical properties of the myocardium.[12)] In this model, by the activated contractile element which stretches a series of elastic elements during systole, the elastic modulus and acoustic impedance inside cells are increased. This process decreases the mismatch in acoustic impedance between the cells and the intercellular substances, resulting in a decrease of the IB value. During diastole, on the other hand, since only the contractile element is extended and the stress and strain applied to the series elastic element become negligible, the acoustic impedance inside the cells is reduced in contrast to the increase during systole. Thus, the mismatch of acoustic impedance between cells and intercellular substances is increased, the IB value is increased, and the cyclic variation of IB reflects the change in the dynamics of the tissue and the pathological change.

It has been reported that ischemia decreases the cyclic variation of IB.[13–18)] One of the factors that affects the cyclic variation of IB is the change in the angle of the ultrasonic beam and the direction of the myocardium fiber.[19–21)] Hall et al. reported that the angle dependence on the backscatter from the intercellular substances with the myocardial cells is equal to that without myocardial cells.[22)] That work showed that the large variation in IB indicates the healthiness of the myocardium. Another factor involved in the decrease in IB cyclic variation due to ischemia is fibrosis of the myocardium.[23)] In severe myocardial fibrosis, the IB value is always high during one cardiac cycle, decreasing its cyclic variation. This phenomenon is thought to be caused by an increase of collagen fiber content and a decrease of systolic function caused by fibrosis of the myocardium. Thus, various research studies have suggested the possibility that the temporal change of IB in the heart wall can be used to assess the myocardial contractile function because it reflects change in the dynamics of tissue, including pathological changes.[24–26)] However, most such studies have not investigated the temporal variations of IB using a high-frame-rate measurement.

In the present study, therefore, the position at which the myocardium was measured was tracked and IB and its temporal variation were obtained at the same site by compensating for movement due to the heartbeat. The IB and its temporal variation had a high temporal resolution of 1.73 ms. Furthermore, the variation of IB during succeeding frames was calculated in order to observe the temporal change of IB. As a result, the regional IB values and the variation of IB during one cardiac cycle for a healthy human heart were obtained. Based on these findings, a hypothesis for its mechanism is proposed in the discussion section.

2. Experimental methods

2.1 Tracking of the heart wall using the phased tracking method

The heart has a translational motion due to the heartbeat, and the contraction and relaxation of the myocardium change the heart wall thickness. For evaluating the IB in each region of interest (ROI) during one cardiac cycle, the measurement position of the myocardium is tracked by suppressing the effect of the translational motion of the heart wall on the measurement of the thickness. In this study, the phased tracking method[27,28] was employed to measure IB at the same site of the heart wall.

Radio frequency (RF) pulses with angular frequency $\omega_0 = 2\pi f_0$ were transmitted at a time interval of ΔT from an ultrasonic transducer on the chest surface. The relationship between the instantaneous distance $x(t)$ of a moving object from the ultrasonic transducer at time t and the instantaneous period $\tau(t)$ required for one-way transmission from the ultrasonic transducer to the object is represented by

$$x(t) = c_0 \cdot \tau(t), \tag{1}$$

where c_0 is the acoustic velocity in the human body. The phase $\theta(x; t)$ of the received signal from the object is given by the angular frequency ω_0 multiplied by twice the delay time $\tau(t)$ in the one-way propagation as follows:

$$\theta(x; t) = 2\omega_0\tau(t) = 4\pi f_0 \frac{x(t)}{c_0}. \tag{2}$$

From this equation, the phase difference $\Delta\theta(x; t)$ between the received signals for the successively transmitted pulses in the interval ΔT is given by

$$\Delta\theta(x; t) = \theta(x; t + \Delta T) - \theta(x; t) = \frac{4\pi f_0}{c_0}\Delta x(t). \tag{3}$$

Therefore, the displacement $\Delta x(t)$ of the object during the period ΔT from a time t is estimated by

$$\Delta x(t) = \frac{c_0}{4\pi f_0}\Delta\theta(x; t). \tag{4}$$

Since this technique enables estimation of the displacement $\Delta x(t)$ of the object with a high degree of accuracy, both ends of the ROI set in each beam are accurately tracked. The position $x(t)$ and the length $\Delta D(t)$ of the ROI are followed in response to translation and thickness change of the heart wall, respectively, and IB is measured in the tracked region as described below by Eq. (6). Furthermore, from $\Delta x(t)$, the average velocity of the object during the period ΔT is given by

$$\hat{v}\left(t + \frac{\Delta T}{2}\right) = \frac{\Delta x(t)}{\Delta T} = c_0 \cdot \frac{\Delta\theta(x; t)}{4\pi f_0 \cdot \Delta T}. \tag{5}$$

This allows estimation of the myocardial velocity at the same site.

2.2 High temporal resolution measurement of IB

As shown in Fig. 1(a), at the time of the R-wave in the electrocardiogram (ECG), measurement layers (ROIs) with a thickness of 616 μm were set along each beam, the interval of the layer centers being 38.5 μm. The displacement of each layer was tracked at both ends of each layer during one cardiac cycle. The IB value of i-th layer (i-th ROI) in the n-th frame, $\mathrm{IB}_i(n)$, was calculated by[29]

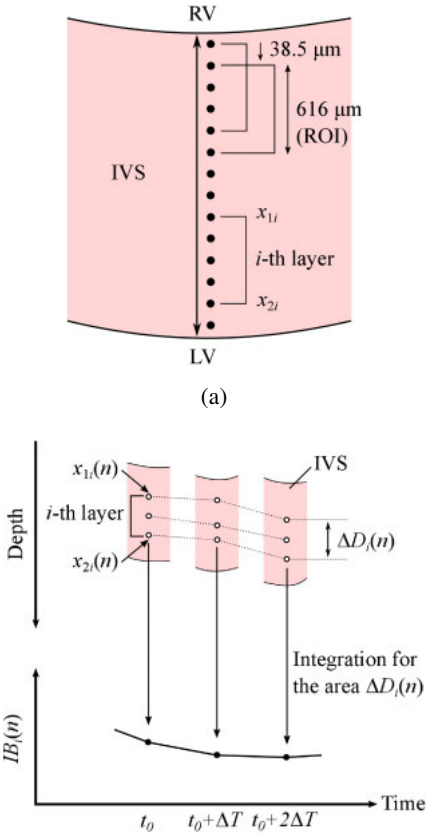

Fig. 1. (Color online) IB measurement at the same site of the myocardium during one cardiac cycle. (a) Setting of the region of interest. (b) Process for estimation of $\mathrm{IB}_i(n)$ for the i-th layer.

$$\mathrm{IB}_i(n) = 10\log_{10}\frac{1}{\Delta D_i(n)}\int_{x_{1i}(n)}^{x_{2i}(n)} |z(n, x)|^2\, dx, \tag{6}$$

where $z(n, x)$ is the received RF signal at a depth x of n-th frame, $x_{1i}(n)$ and $x_{2i}(n)$ are the positions of the upper and lower ends of i-th layer in n-th frame, and $\Delta D_i(n) = x_{2i}(n) - x_{1i}(n)$ is the length of i-th layer (i-th ROI) in the depth direction, as shown in Fig. 1(b).

Furthermore, the variation of IB among succeeding frames was evaluated in order to observe the temporal change of IB. The calculated IB contains many high-frequency components, which may originate from time variance in the amplitude of the reflected signal and in the estimation of the length of the layer in Eq. (6). To suppress the high-frequency components of the IB waveform, time averaging of the IB waveform was applied with Hanning window $w(n)$ given by

$$w(n) = 0.5 - 0.5\cos\left(\frac{2\pi n}{N}\right) \quad (n = 0, 1, \ldots, N-1), \tag{7}$$

where N is the length of the Hanning window, that is, the IB waveform is averaged during N frames. Furthermore, using the averaged IB, $\overline{\mathrm{IB}}_i(n)$, the variation of IB, $\Delta\mathrm{IB}_i(n)$, was obtained by

$$\Delta\mathrm{IB}_i(n) = \frac{1}{\Delta T} \times \{\overline{\mathrm{IB}}_i(n) - \overline{\mathrm{IB}}_i(n-1)\}. \tag{8}$$

2.3 Experimental setting

Using an ultrasonic diagnostic device (Hitachi-Aloka ProSound F75) with a 3 MHz sector probe (Hitachi-Aloka

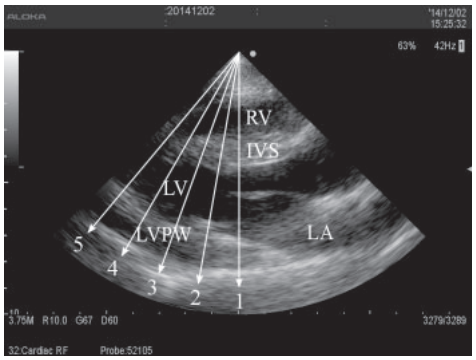

Fig. 2. Five ultrasonic beams were set in the parasternal long-axis ultrasound image of the heart of a 22-year-old healthy male subject. Right ventricular (RV), interventricular septum (IVS), left ventricular (LV), left ventricular posterior wall (LVPW), and left atrium (LA).

UST-52105), RF signals were acquired in a parasternal long-axis ultrasonic image of the heart of a 22-year-old healthy male. Figure 2 shows the B-mode image of the heart of the subject. Five ultrasonic beams were sparsely set every 10° and scanned to achieve a high temporal resolution of a 579-Hz-frame rate ($\Delta T = 1.73$ ms). The IB value of the i-th layer in n-th frame, $\mathrm{IB}_i(n)$, of Eq. (6) was obtained, and by averaging $\mathrm{IB}_i(n)$ with a Hanning window of a 71-ms width of Eq. (7), the averaged IB, $\overline{\mathrm{IB}}_i(n)$, was obtained. Finally, the variation of IB, $\Delta\mathrm{IB}_i(n)$, of Eq. (8) was estimated at a frame interval of $\Delta T = 1.73$ ms.

3. Results and discussion

Figure 3 shows the variation of IBs, $\{\Delta\mathrm{IB}_i(n)\}$, along beam 3 in the IVS and LVPW of Fig. 2 during one cardiac cycle superimposed on a M-mode image. In the latter half of diastole, the sign of the variation of IBs, $\{\Delta\mathrm{IB}_i(n)\}$, changed synchronously across the IVS and LVPW, where the change cycle was about 60–100 ms. Figure 4 shows the averaged IBs, $\{\overline{\mathrm{IB}}_i(n)\}$, at three different depths in the IVS, as shown in the striped pattern which appeared in the variation of IBs, $\{\Delta\mathrm{IB}_i(n)\}$, in Fig. 3, that is, in the latter half of diastole from 0.60 to 1.03 s, and Fig. 5 shows the change in thickness of the IVS in the corresponding period. The peaks and dips of averaged IB waveforms, $\{\overline{\mathrm{IB}}_i(n)\}$, appeared almost simultaneously at all depths. Since the thickness change of each measurement layer was smaller than the wavelength ($\lambda = 500\,\mu$m), as shown in Fig. 5, the averaged IB values, $\{\overline{\mathrm{IB}}_i(n)\}$, in Fig. 4 changed even when a change in thickness in Fig. 5 was sufficiently small compared with the wavelength. Thus, the cause of the variation of IBs, $\{\Delta\mathrm{IB}_i(n)\}$, in Fig. 3(a) cannot be explained only by the change in thickness.

The main scatterers in myocardium are the collagen fibers that surround the myocardium fibers, as shown in Fig. 6. The myocardium has a layer structure, each layer of which consists of three or four myocardium fibers (70–100 μm), and the layer boundaries (0–50 μm) include an abundance of collagen fibers.[30] Therefore, the layer interval is about 100 μm, which corresponds to an interval is about $\lambda/5$ in the present study ($\lambda = 500\,\mu$m).

Figure 7 shows a model of the change in IB originating in the change in thickness. When scatterers of identical size are distributed regularly at a constant interval of $\Delta x = 100\,\mu$m, as

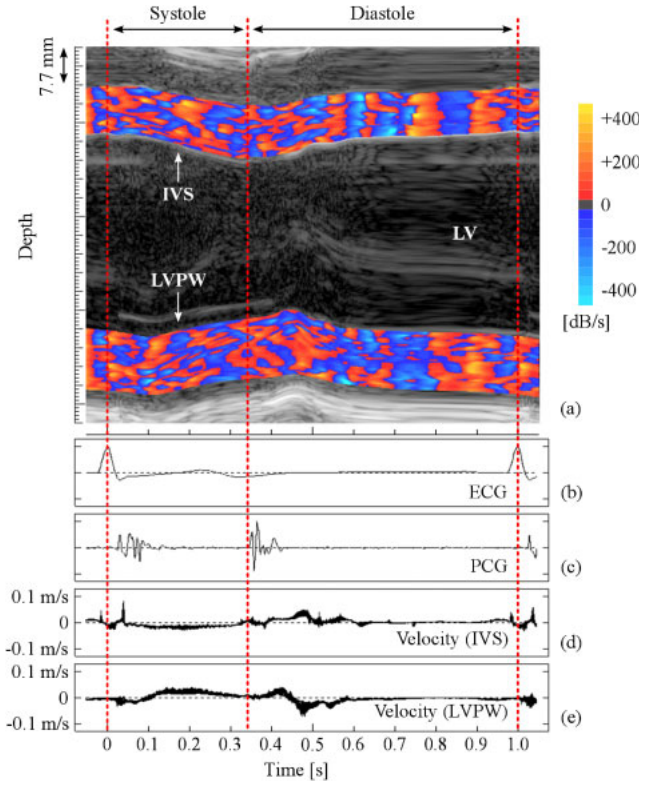

Fig. 3. (Color online) Variation of IB, $\{\Delta\mathrm{IB}_i(n)\}$, during one cardiac cycle in the IVS and LVPW. (a) Variation of IB, $\{\Delta\mathrm{IB}_i(n)\}$, along beam 3 superimposed on an M-mode image. (b) ECG. (c) Phonocardiogram (PCG). (d) Velocity waveform $v_i(t)$ of each point in the IVS. (e) Velocity waveform $v_i(t)$ of each point in the LVPW.

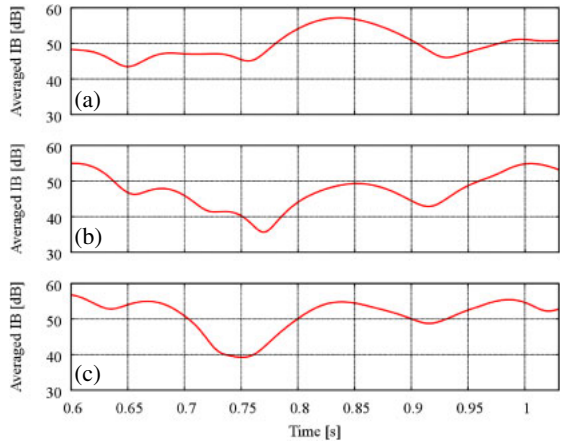

Fig. 4. (Color online) Averaged IB signal in the IVS. (a) RV side, (b) middle, and (c) LV side.

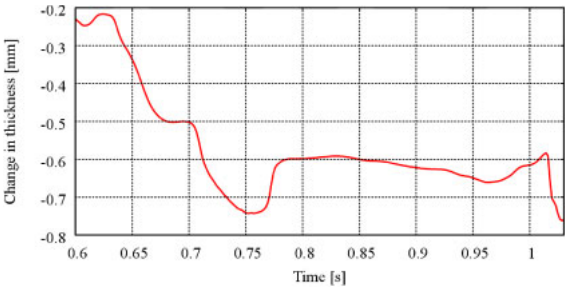

Fig. 5. (Color online) Change in thickness during the latter half of diastole in the IVS.

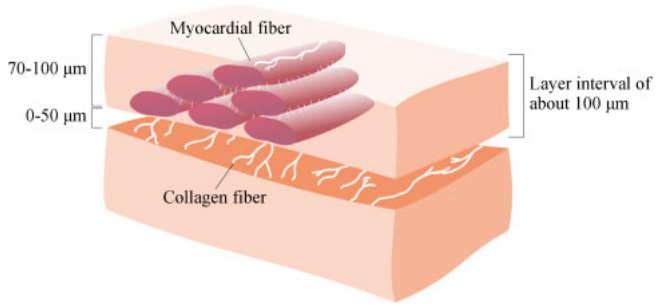

Fig. 6. (Color online) An illustration of layered structure of the myocardium.

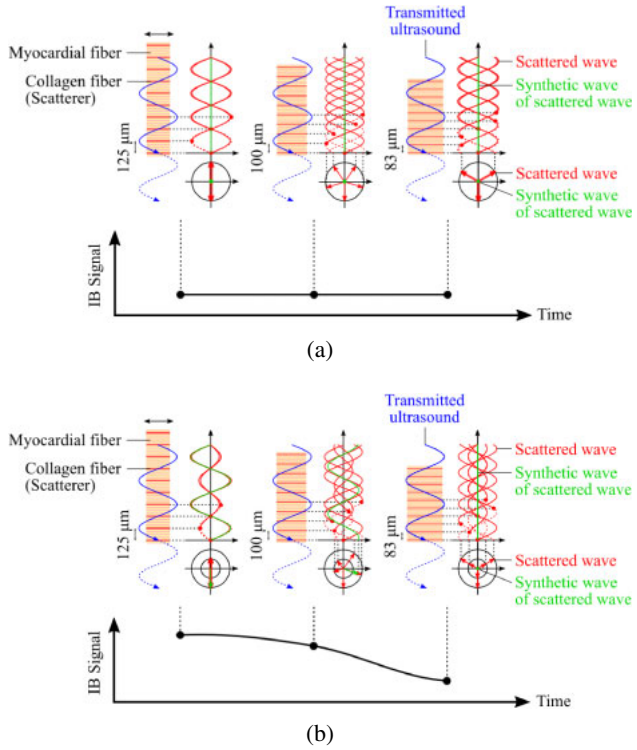

Fig. 7. (Color online) A model showing dependence of the relationship between change in the interference state of the scattered waves and the IB value on change in thickness in the myocardium when scattering intensities of the scatterers are uniform (a) and non-uniform (b).

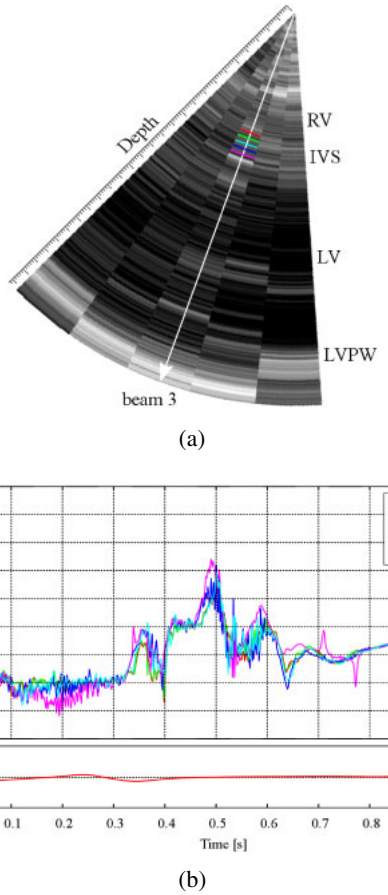

Fig. 8. (Color online) Displacement $\Delta x(t)$ of Eq. (4) during one cardiac cycle at five different depths in the IVS of the same human subject. (a) Positions of five different depths in the B-mode image with space scan. (b) Displacement waveform $\Delta x_i(t)$.

shown in Fig. 7(a), the scattered echoes cancel each other out regardless of the contraction ($\Delta x = 125\,\mu$m) and relaxation ($\Delta x = 83\,\mu$m) of the myocardium, resulting in a low IB value at almost all times. In contrast, when scatterers of different size are distributed at different intervals, as shown in Fig. 7(b), a slight change in the tissue thickness varies the interference state of the echoes from scatterers, resulting in a large change in IB. Since the change in thickness during the latter part of diastole in Fig. 3(a) is sufficiently smaller than $\lambda/2$, as shown in Fig. 5, the change of IB values may be caused by the process shown in Fig. 7(b).

According to the above model, it can be explained that the synchronized variation of IBs, $\{\Delta \mathrm{IB}_i(n)\}$, across the heart wall in Fig. 3(a) occurs by the synchronized contraction and relaxation across the heart wall. Figure 8(b) shows the displacements $\{\Delta x_i(n)\}$ in the myocardium of the myocardial layers during one cardiac cycle at five different depths set in the IVS, as shown in Fig. 8(a). The difference among the displacements $\{\Delta x_i(n)\}$ of five layers became relatively small after 0.6 s in the slow filling and the atrial systole phases. It can be said that all the myocardial fiber layers across the heart wall showed similar motion. In these phases, the left ventricular volume greatly increased and then the left ventricular pressure slightly increased. Since the sarcomere length is constant in these phases,[31] the averaged IBs, $\{\overline{\mathrm{IB}}_i(n)\}$, in these phases observed in Fig. 4 may originate from the minute thinning of the myocardium across the heart wall caused by the increase of the ventricular volume.

This assumption was confirmed by the following experiment using a bovine heart. As shown in Fig. 9, the IVS of a bovine heart with a length of 90 mm and a thickness of 35 mm was extracted and fixed in a water tank with physiological saline solution of 0.9% concentration at 23 °C. Similar to the parasternal long-axis image of the human heart, the IVS was fixed so that the right ventricular side was set at the upper side and the left ventricular side was set at the lower side. Since the left ventricular volume increases about 1.5 times in the slow filling phase and the atrial systole phase, the IVS lengthens by about $1.14 = \sqrt[3]{1.5}$ times. Thus, the extracted IVS of the bovine should be stretched at least by 13 mm, which corresponds to 14% of the 90 mm length of the IVS. In the actual experiment, it was stretched by 20 mm. By setting both ends of the IVS to the arms of a stage controller using forceps, one side of the IVS was stretched by 20 mm for 4 s at a constant speed, resulting

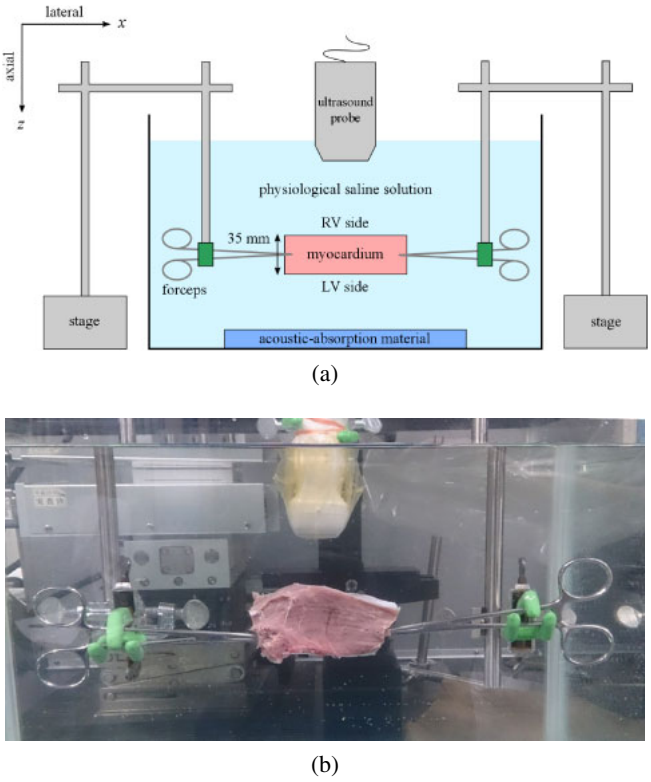

Fig. 9. (Color online) IB measurement of the IVS of the bovine heart. (a) Experimental system. (b) State of measurement.

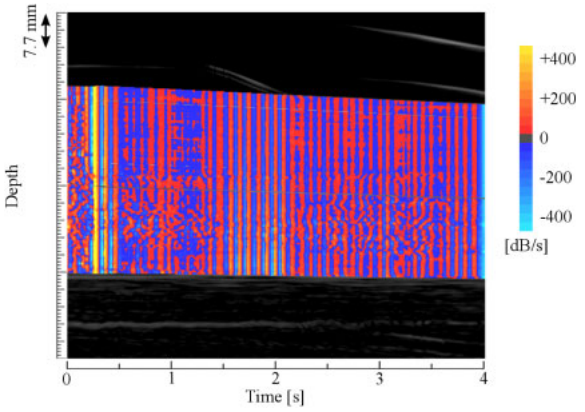

Fig. 10. (Color online) Variation of IB, $\{\Delta IB_i(n)\}$, in the IVS of the bovine heart in Fig. 9.

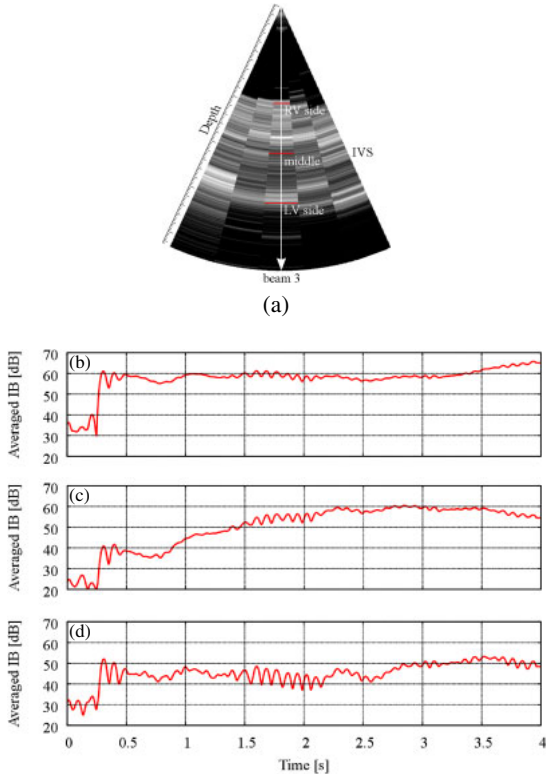

Fig. 11. (Color online) Averaged IB signal in the IVS of the bovine heart in Fig. 9 at three different typical layers. (a) Positions of three different depth layers. Averaged IB signals, $\{\overline{IB}_i(n)\}$, for (b) RV side, (c) middle, and (d) LV side.

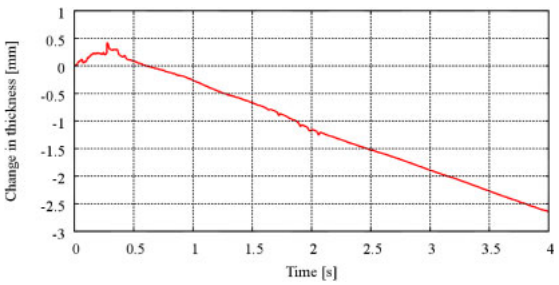

Fig. 12. (Color online) Change in thickness in the IVS of the bovine heart in Fig. 9.

in a decrease in thickness of 2.7 mm. Using the same ultrasonic diagnostic device and method as applied to the human heart in Fig. 3, the averaged IB values, $\{\overline{IB}_i(n)\}$, and the variation of IBs, $\{\Delta IB_i(n)\}$, were obtained, as shown in Figs. 10 and 11, respectively.

Figure 10 shows the variation of IBs, $\{\Delta IB_i(n)\}$, in the IVS for 4 s superimposed on the M-mode image. A striped pattern was clearly observed and the variation of IBs, $\{\Delta IB_i(n)\}$, changed synchronistically across the bovine heart wall, similar to what occurred in the in vivo measurement in Fig. 3(a). Figures 11(b)–11(d) show averaged IB waveforms, $\{\overline{IB}_i(n)\}$, for three different depth layers set along the ultrasonic beam in the bovine IVS, as shown in Fig. 11(a), and Fig. 12 shows the change in thickness of the IVS. As shown in Fig. 12, the thickness decreased almost linearly. Though the thickness change of each measurement layer was much smaller than the wavelength, the peaks and dips of averaged IB waveforms, $\{\overline{IB}_i(n)\}$, appeared almost simultaneously across the heart wall. These results are consistent with the in vivo measurement shown in Figs. 3(a) and 5(b)–5(d). Since this experiment using a bovine heart simulated the thinning of the human IVS in the slow filling and atrial systole phases, the change in the averaged IB values, $\{\overline{IB}_i(n)\}$, in slow filling and the atrial systole phases of the human IVS can be explained as being due to the change in the positions of non-uniform scatterers associated with the thickness change smaller than the wavelength.

4. Conclusions

In this study, the measurement position of the myocardium was tracked and IB and its temporal variation were obtained from the same site by compensating for the movement due to the heartbeat. The IB and its temporal variation have a high

temporal resolution of 1.73 ms. The peaks and dips of IB waveforms appeared almost simultaneously across all depths during the slow filling and atrial systole phases. Also, the thickness change of each measurement layer was much smaller than the wavelength. Therefore, by modeling the change in interference state of the echoes from scatterers and IB values originating from the thickness of the myocardium, non-uniformity of the scattering intensity of the scatter was shown. Furthermore, the reason for the occurrence of the synchronized variation of IB across the heart wall during contraction and relaxation was found by an experiment using the bovine heart. These new findings show that the IB value reflects a small movement of the myocardium of about 5 mm/s, showing the potential of using IB measurement to evaluate contraction and relaxation of the myocardium quantitatively and accurately.

1) A. K. Bhandari and N. C. Nanda, Am. J. Cardiol. **51**, 817 (1983).
2) J. G. Miller, J. E. Perez, and B. E. Sobel, Prog. Cardiovasc. Dis. **28**, 85 (1985).
3) H. Yoshiara, H. Hasegawa, H. Kanai, and M. Tanaka, Jpn. J. Appl. Phys. **46**, 4889 (2007).
4) R. Omoto, Y. Yokote, S. Takamoto, S. Kyo, K. Ueda, H. Asano, K. Namekawa, C. Kasai, Y. Kondo, and A. Koyano, Jpn. Heart J. **25**, 325 (1984).
5) J. F. Pombo, B. L. Troy, and R. O. Russell, Circulation **43**, 480 (1971).
6) J. W. Mimbs, D. Bauwens, R. D. Cohen, M. O'Donnell, J. G. Miller, and B. E. Sobel, Circ. Res. **49**, 89 (1981).
7) M. O'Donnell, D. Bauwens, J. W. Mimbs, and J. G. Miller, Proc. IEEE Ultrason. Symp., 1979, p. 175.
8) J. W. Mimbs, M. O'Donnell, D. Bauwens, J. G. Miller, and B. E. Sobel, Circ. Res. **47**, 49 (1980).
9) J. W. Mimbs, M. O'Donnell, J. G. Miller, and B. E. Sobel, Am. J. Cardiol. **47**, 1056 (1981).
10) R. M. Hoyt, D. J. Skorton, S. M. Collins, and H. E. Melton, Jr., Circulation **69**, 775 (1984).
11) E. I. Madaras, B. Barzilai, J. E. Perez, B. E. Sobel, and J. G. Miller, Ultrason. Imaging **5**, 229 (1983).
12) S. A. Wickline, L. J. Thomas, III, J. G. Miller, B. E. Sobel, and J. E. Perez, J. Clin. Invest. **76**, 2151 (1985).
13) B. Barzilai, E. I. Madaras, B. E. Sobel, J. G. Miller, and J. E. Perez, Am. J. Phys. **247**, 478 (1984).
14) J. G. Mottley, R. M. Glueck, J. E. Perez, B. E. Sobel, and J. G. Miller, J. Acoust. Soc. Am. **76**, 1617 (1984).
15) M. R. Milunski, G. A. Mohr, J. E. Pérez, Z. Vered, K. A. Wear, C. J. Gessler, B. E. Sobel, J. G. Miller, and S. A. Wickline, Circulation **80**, 491 (1989).
16) R. H. Hoyt, S. M. Collins, D. J. Skorton, E. E. Ericksen, and D. Conyers, Circulation **71**, 740 (1985).
17) T. Masuyama, F. G. St. Goar, T. L. Tye, G. Oppenheim, I. Schnittger, and R. L. Popp, Circulation **80**, 925 (1989).
18) Z. Vered, B. Barzilai, G. A. Mohr, L. J. Thomas, R. Genton, B. E. Sobel, T. A. Shoup, H. E. Melton, J. G. Miller, and J. E. Pérez, Circulation **76**, 1067 (1987).
19) E. I. Madaras, J. Perez, B. E. Sobel, J. G. Mottley, and J. G. Miller, J. Acoust. Soc. Am. **83**, 762 (1988).
20) J. G. Mottley and J. G. Miller, J. Acoust. Soc. Am. **83**, 755 (1988).
21) M. R. Holland, U. M. Wilkenshoff, A. E. Finch-Johnston, S. M. Handley, J. E. Perez, and J. G. Miller, J. Am. Soc. Echocardiogr. **11**, 929 (1998).
22) C. H. Hall, M. J. Scott, G. M. Lanza, J. G. Miller, and S. A. Wickline, J. Acoust. Soc. Am. **107**, 612 (2000).
23) J. Naito, T. Masuyama, T. Mano, H. Kondo, K. Yamamoto, R. Nagano, Y. Doi, M. Hori, and T. Kamada, Am. Heart J. **131**, 115 (1996).
24) S. A. Wickline, L. J. Thomas, III, J. G. Miller, B. E. Sobel, and J. E. Perez, Circulation **74**, 389 (1986).
25) S. Nozaki, A. N. DeMaria, G. A. Helmer, and H. K. Hammond, Circulation **92**, 2676 (1995).
26) S. Takiuchi, H. Ito, K. Iwakura, Y. Taniyama, N. Nishikawa, T. Masuyama, M. Hori, Y. Higashino, K. Fujii, and T. Minamino, Circulation **97**, 356 (1998).
27) H. Kanai, M. Sato, Y. Koiwa, and N. Chubachi, IEEE Trans. Ultrason. Ferroelectr. Freq. Control **43**, 791 (1996).
28) H. Kanai, N. Chubachi, Y. Koiwa, and M. Tanaka, IEEE Trans. Ultrason. Ferroelectr. Freq. Control **44**, 752 (1997).
29) H. Kanai, Y. Koiwa, S. Katsumata, N. Izumi, and M. Tanaka, Jpn. J. Appl. Phys. **42**, 3239 (2003).
30) I. J. LeGrice, B. H. Smaill, L. Z. Chai, S. G. Edgar, J. B. Gavin, and P. J. Hunter, Am. J. Phys. **296**, 571 (1995).
31) E. K. Rodriguez, W. C. Hunter, M. J. Royce, M. K. Leppo, A. S. Douglas, and H. F. Weisman, Am. J. Phys. **263**, 293 (1992).